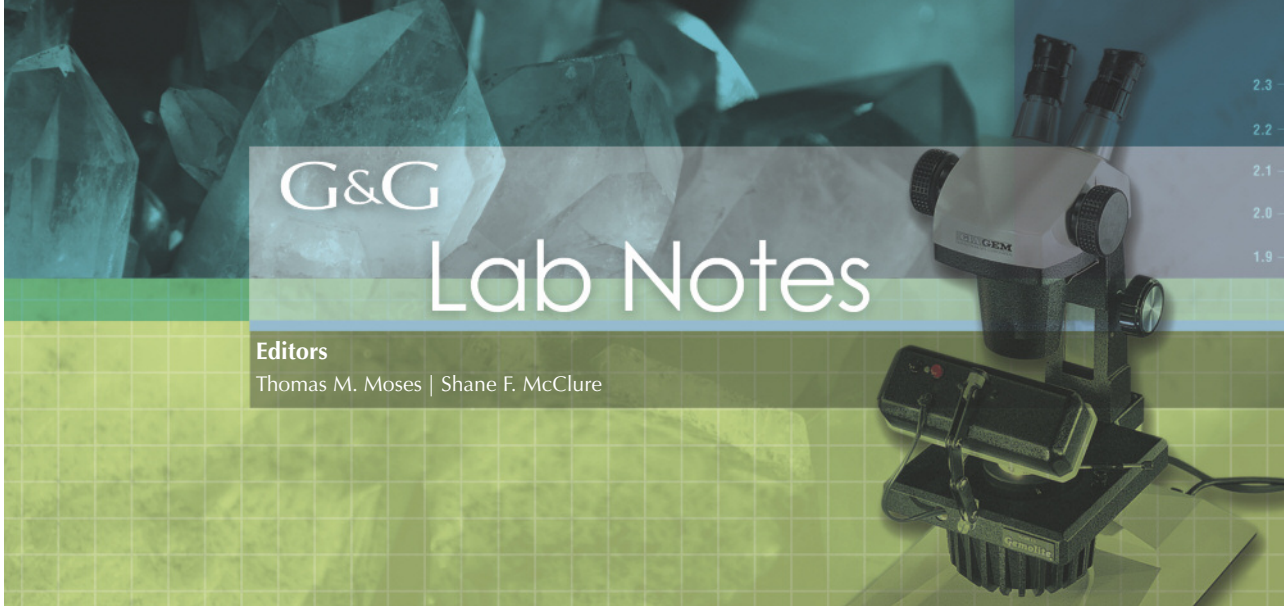


## Graphite Inclusions Forming Octahedral Outline in DIAMOND

Primary diamond deposits are usually found in mantle-derived igneous rocks, with the principal hosts being kimberlite and lamproite. During the ascent to the earth's surface, diamonds may be converted, partially or entirely, to graphite and chemically dispersed and eliminated (A.A. Snelling, "Diamonds – Evidence of explosive geological processes," *Creation*, Vol. 16, No. 1, 1993, pp. 42–45). GIA's New York laboratory recently received a 1.30 ct Fancy brownish greenish yellow diamond (figure 1) containing an octahedral-shaped inclusion outlined by minute crystal inclusions along the junctions of the crystal faces.

Gemological examination at 60× magnification reveals that the octahedral-shaped inclusion is outlined by numerous irregular dark crystals (figure 2). Advanced gemological analysis with UV-Vis and FTIR spectroscopy confirmed that this was a natural diamond with a natural color origin.

Further analysis using Raman spectroscopy reveals that the dark inclusions are graphite crystals with a Raman peak at 1590 $cm^{-1}$ (figure 3), which corresponds to the graphite G band (I. Childres et al., "Raman spectroscopy of graphene and related materials," in J.I. Jang, Ed., *New Developments in Photon and Materials Research*, Nova Science Publications, 2013). Since this G band is at a slightly higher energy level than that from the primary graphite, which usually peaks at around 1580 $cm^{-1}$, we propose that the crystals tested are likely the secondary graphite converted from part of the original diamond into graphite form during the specific growth episode when oxidized fluids rich in $CO_2$ and $H_2O$ passed through diamond bearing horizons. This also explains the shift of the G band to a higher energy, due to the higher strain near these newly formed secondary graphite crystals (J. Hodkiewitcz, "Characterizing graphene with Raman spectroscopy," *Application Note: 51946*, Thermo Fisher Scientific, Madison, Wisconsin, 2010). Late formation of additional diamond layers on top of the graphites would have converted them to covered internal features within the larger diamond (R.H. Mitchell, *Kimberlites and Lamproites: Primary Sources of Diamond*, Geoscience Canada Reprint Series 6, Vol.

*Figure 1. This 1.30 ct Fancy brownish greenish yellow diamond contains an octahedral-shaped inclusion.*

*Figure 2. Minute graphite inclusions outline the octahedral crystal faces in this diamond. Field of view 7.19 mm.*

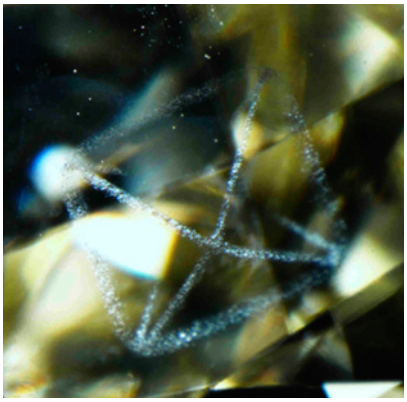

*Editors' note: All items were written by staff members of GIA laboratories.*

Gems & Gemology, Vol. 51, No. 4, pp. 428–440.

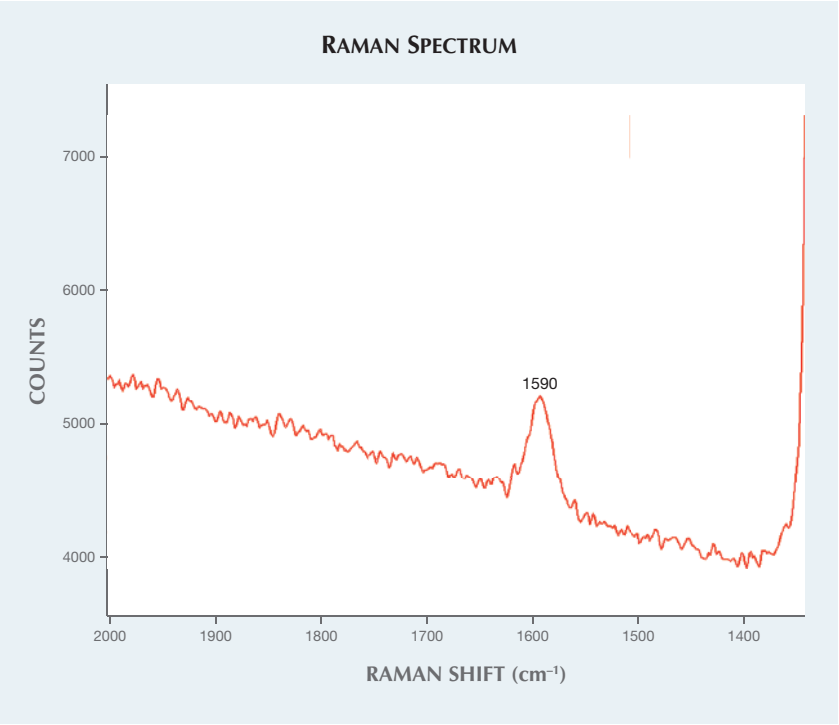


*Figure 3. The graphite G band at 1590 cm$^{-1}$ is found on the minute crystals along the crystal junctions, confirming that they are graphite crystals.*

18, No. 1, 1991, pp. 1–16). Primary graphite crystals could also mix into the crystal clouds during the diamond's growth due to changes in environmental temperature, pressure, and the growth fluid's chemical elements. These minute graphite crystals would tend to form along the junctions of crystal faces, since they usually have a higher surface energy. Thus, we believe that both primary and secondary graphite formation, occurring between the diamond's growth episodes, contributed to this phenomenal octahedral outline.

Graphite inclusions are commonly seen in diamonds as isolated crystals or jointed crystal clouds. It is very unusual to see these minute graphite inclusions formed at the junctions of the original diamond crystal faces and outlining the octahedral growth pattern. This stone not only captures the amount of stress and extreme conditions under which the diamond grew, but also shows the beauty of the formation of crystalline diamond.

*Yixin (Jessie) Zhou*

## Treated Pink with HPHT Synthetic Growth Structure

HPHT synthetic diamonds are grown using high pressure and high temperature but with a much higher growth rate than natural diamond. Consequently, their growth structures are different. GIA's New York lab recently examined a multi-step treated diamond with a growth structure similar to that of HPHT synthetics. The 1.62 ct Fancy pink type IIa round brilliant seen in figure 4 showed spectral characteristics suggestive of HPHT treatment, irradiation, and annealing. This diamond was internally clean, except for the presence of strong, colorless internal graining (figure 5). Tatami and banded strains with strong interference colors could be seen under cross-polarized light (again, see figure 5). Based on these microscopic features, we concluded that this was a natural diamond.

DiamondView imaging of the stone showed cuboctahedral growth with dark sectors and pink coloration (figure 6). This crystal habit is usually observed in HPHT-grown synthetic diamonds. As seen in figure 6 (left), the cubic {100} sector can be located in the pavilion, along with octahedral {111} sectors. In order to understand more about this growth, we compared it with a type IIa 0.27 ct HPHT synthetic, which was treated post-growth to induce a Fancy Intense orangy pink color (figure 6, right). Both specimens showed similar fluorescence patterns; however, the natural diamond's greenish blue phosphorescence was evenly distributed, as seen in the middle image of figure 6. This is unlike the dark images yielded from type IIa pink HPHT synthetics, which are not phosphorescent.

Although most natural diamonds show octahedral growth structure in DiamondView images, some natural gem-quality colorless and yellow diamonds may show cuboctahedral growth (Winter 2010 Lab Notes, pp. 298–299; Winter 2011 Lab Notes, p. 310; Spring 2013 Lab Notes, pp. 45–46). Some non-gem-quality diamonds possess cuboctahedral form (D.G. Pearson et al., "Orogenic ultramafic rocks of UHP (diamond facies) origin," in R.G. Coleman and X. Wang, Eds., *Ultrahigh Pressure Metamorphism*, Cambridge University Press, 1995, pp. 456–510). Growth rate, pressure, and temperature of geological environment control the habit of a di-

*Figure 4. This multi-step treated 1.62 ct Fancy pink natural diamond shows what appears to be HPHT synthetic growth structure.*

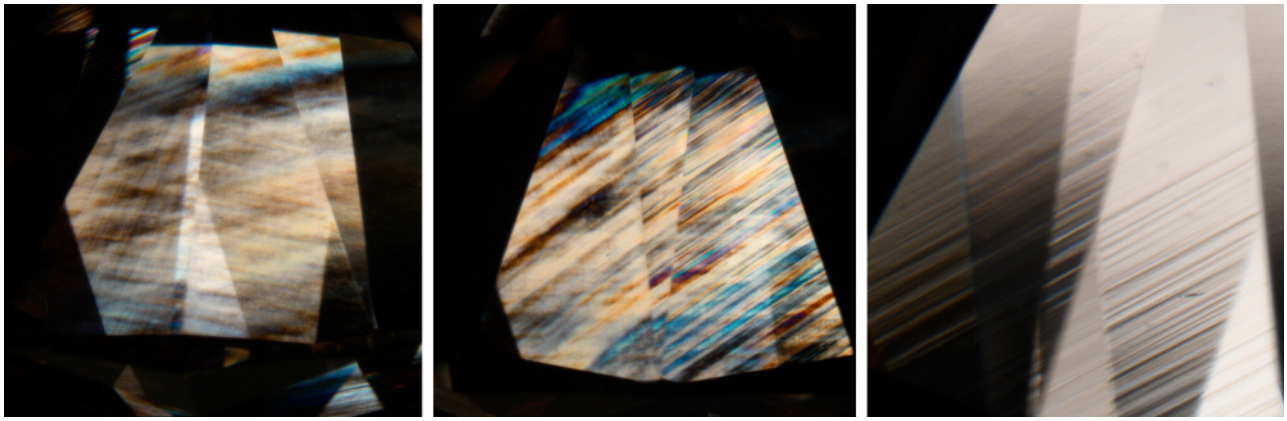

*Figure 5. Tatami strain (left, field of view 3.20 mm), banded strain (middle, field of view 3.20 mm), and heavy internal graining (right, field of view 2.45 mm) are evidence of a natural diamond.*

amond crystal. A slow growth rate causes octahedral crystal growth, but a high growth rate can facilitate cubic {100} and octahedral {111} sectors developing simultaneously. As a result, cuboctahedral habit can be formed naturally.

While the DiamondView is very reliable at revealing the growth structure of natural vs. synthetic diamond, it is important to correctly interpret all identifying characteristics. When cuboctahedral growth structure is observed, one should look for other features to support the origin. Microscopic features and spectral characteristics are useful for this purpose.

*Kyaw Soe Moe and Wuyi Wang*

## Very Large Type Ib Natural Diamond

Nitrogen is the main impurity in diamond and during growth it is initially incorporated in the diamond lattice as isolated nitrogen atoms (C centers). Diamonds where the majority of nitrogen occurs in C centers are known as type Ib. While C centers are common in lab-grown HPHT diamonds, the occurrence of C centers in natural cratonic diamonds is extremely rare (<1% of all natural diamonds). Natural diamonds form deep in Earth's mantle, where high temperatures result in nitrogen aggregating to form A centers ($N_S$) and B centers ($N_4V$).

GIA's New York laboratory recently tested a large 13.09 ct gem-quality natural type Ib rough diamond. The diamond measured 13.51 × 11.56 × 10.18 mm, with rounded dodecahedral morphology and clear dissolution pits on some faces in a symmetrical pattern (figure 7). The diamond had a highly saturated, slightly orangy yellow color evenly distributed throughout the whole crystal. The diamond contained two tiny sulfide inclusions with their associated graphitic rosette fracture systems.

The infrared absorption spectrum revealed typical features of natural type Ib diamonds: a sharp peak at 1344 $cm^{-1}$ and a broad band at 1130 $cm^{-1}$. The absorption attributed to the

*Figure 6. DiamondView fluorescence images of the treated 1.62 ct pink natural (left) and the post-growth treated 0.27 ct pink HPHT synthetic (right) showed similar growth patterns, containing cubic {100} sector and octahedral {111} sectors. The middle image of phosphorescence of the 1.62 ct pink natural diamond showed even color distribution without growth sectors. Type IIa pink HPHT synthetic diamonds are usually not phosphorescent.*

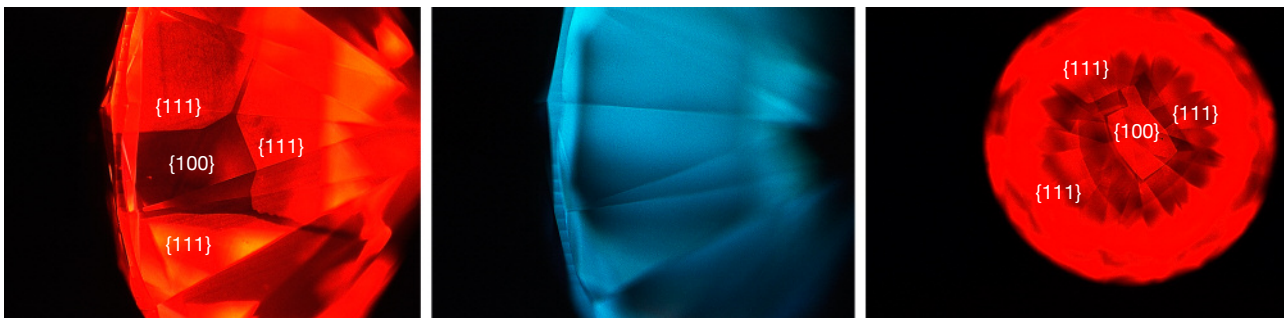

*Figure 7. The yellow color of this gem-quality 13.09 ct type Ib natural diamond rough is due to the presence of isolated nitrogen (C centers).*

A center (1280 $cm^{-1}$) was rather weak. Spectral fitting showed that 75% of the nitrogen existed as C centers and 8% as A centers. This diamond did not contain any amber centers, which is consistent with the lack of plastic deformation lines or brownish hue.

The UV-Vis-NIR absorption spectrum, collected at liquid nitrogen temperature, showed a smooth and gradual increase in absorption from the near-infrared region to about 560 nm, and then a sharp increase to the high-energy side. C centers were the only color-introducing defect in this large diamond.

Photoluminescence (PL) spectra were collected at liquid nitrogen temperature with various laser excitations. Under 514 nm laser excitation, $[N\text{-}V]^0$ at 574.9 nm and $[N\text{-}V]^-$ at 637.0 nm were detected. Many sharp emissions with unknown assignments were also observed (figure 8). With 830 nm laser excitation, weak emissions at 882/884 nm from Ni-related defects were observed.

Large type Ib diamonds with intense yellow color are rarely seen. GIA continues to study these rare diamonds to understand the geological processes that allow isolated nitrogen to be preserved in some natural diamonds. Preservation of C centers in these natural diamonds is typically attributed to very young formation ages or to storage of these diamonds at cooler temperatures in Earth's mantle than most other diamonds. Ongoing isotopic age dating of sulfide inclusions, combined with temperature constraints, will provide the opportunity to evaluate how these enigmatic type Ib diamonds are preserved in natural cratonic settings.

*Wuyi Wang and Karen Smit*

## Uranium Contents of HYALITE

Hyalite is a colorless variety of common opal with strong greenish fluorescence. Rough specimens have interesting glassy botryoidal shapes formed by vapor transport in volcanic or pegmatitic environments (O.W. Flörke, "Transport and deposition of $SiO_2$ with $H_2O$ under supercritical conditions," *Kristall und Technik*, Vol. 7, 1972, pp. 159–166). Hyalite from a new source in Zacatecas, Mexico, discovered in 2013, shows strong green fluorescence even under daylight conditions. This material was spotlighted for the first time at the 2014 Tucson gem and mineral shows (E. Fritsch et al., "Green-luminescing hyalite opal from Zacatecas, Mexico," *Journal of Gemmology*, Vol. 34, 2015, pp. 490–508).

GIA's Tokyo laboratory recently had an opportunity to examine several faceted hyalites from Zacatecas, Mexico, along with several rough hyalites from other locations, including Japan, Hungary, and Argentina. There were two different types of Japanese hyalites in the study samples: botryoidal and spherical. The botryoidal one (figure 9) was from Gifu's Naegi granitic pegmatite (H. Ogawa et al., "Fluorescence of hyalite in pegmatite from Naegi granite, Nakatugawa," 2008 Annual Meeting of Japan Association of Mineralogical Sciences), while the spherical one was from Toyama's Shin-yu hot spring (Y. Takahashi et al., "On the occurrence of opal at the Shin-yu hot spring, Tateyama," *Tateyama Caldera Research*, Vol. 8, 2007, pp. 1–4.). Hungarian hyalite is known to form in the clefts of trachytic rocks in Bohemia, Czech Republic, and Auvergne, France (B. von Cotta, *Rocks Classified and Described: A Treatise on Lithology,* Longmans, Green, and Company, London, 1866, p. 425). Argentinean hyalite is widely distributed, but the original rocks are not described.

*Figure 8. The diamond's PL spectrum, collected at liquid nitrogen temperature with 514 nm laser excitation, showed emissions related to N-V centers along with many sharp peaks of unknown assignment.*

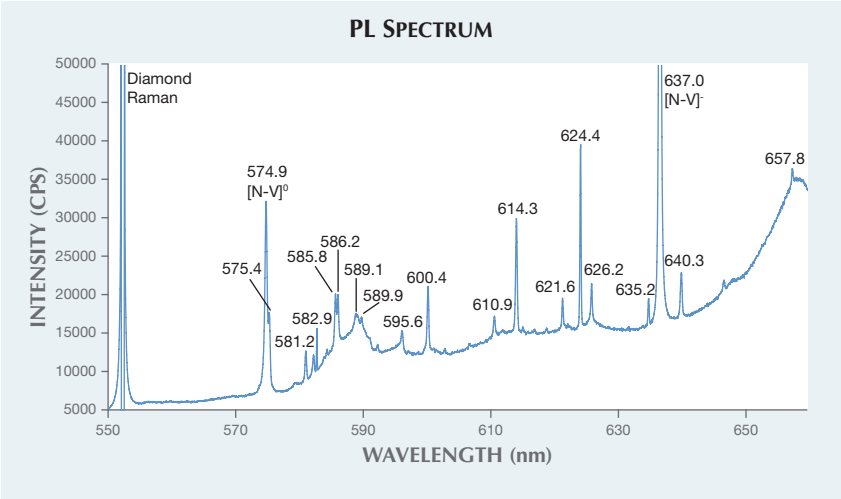

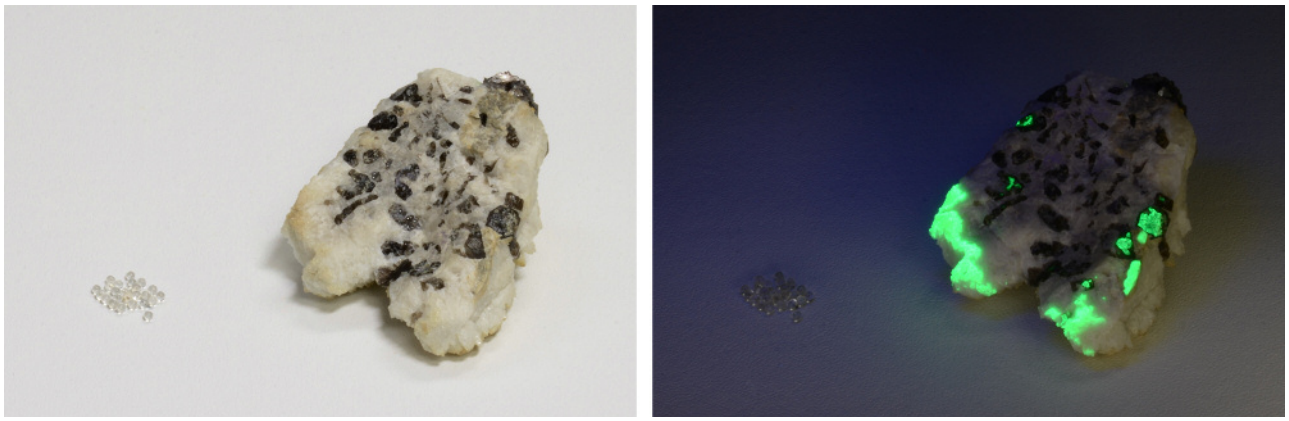

*Figure 9. Two different types of Japanese hyalite rough specimens under daylight (left) and short-wave UV light (right). The photo on the right demonstrates the strong yellow-green fluorescence of pegmatite hyalite, while the spherical hyalite samples do not show the fluorescence.*

Standard gemological testing of the faceted Mexican stones revealed RI values of 1.460–1.461 and a hydrostatic SG of 2.13. Prominent fluorescence was observed under short-wave UV light, but only the Japanese spherical samples were inert (figure 10). Strong graining flow structures were visible at 64× magnification. Raman analysis (figure 11) revealed typical amorphous silica spectra composed of a major band between 430 and 460 $cm^{-1}$ (vibration of bridging oxygen) and a band centered at 790 $cm^{-1}$ representing the stretching of isolated $SiO_4^{4-}$ (P. McMillan, "A Raman spectroscopic study of glasses in the system CaO-MgO-$SiO_2$," *American Mineralogist*, Vol. 69, 1984, pp. 645–659). Laser ablation–inductively coupled plasma–mass spectrometry (LA-ICP-MS) detected a very wide range of uranium contents; the maximum was 1060–1330 ppmw for the Japanese pegmatitic hyalite, while the Japanese spherical hyalite had zero uranium content. The amounts are quite inhomogeneous, but seem to correlate with the intensities of fluorescence, decreasing from Mexican (1180–3.55 ppmw) to Argentinian (2.48–2.49 ppmw) to Hungarian (0.39–0.15 ppmw) (figure 11). Interestingly, only the Japanese pegmatitic hyalite sample was rich in rare earth elements (REE). Since Naegi granitic pegmatite is known to be an REE-enriched pegmatite (T.S. Ercit, "REE-enriched granitic pegmatites," in R.L. Linnen and I.M. Samson, Eds., *Rare-Element Geochemistry and Mineral Deposits*, Geological Association of Canada, GAC Short Course Notes 17, 2005, pp. 175–199), the host rock chemistry appears to affect the silica-rich fluid.

*Figure 10. Clockwise from top center, one Hungarian botryoidal hyalite with matrix, one Japanese pegmatite rough hyalite with matrix, twenty-three pieces of Japanese spherical hyalite, one rough and three faceted Mexican specimens, and one Argentinian botryoidal hyalite under short-wave UV light. The intensity of yellow-green fluorescence vary in the different specimens.*

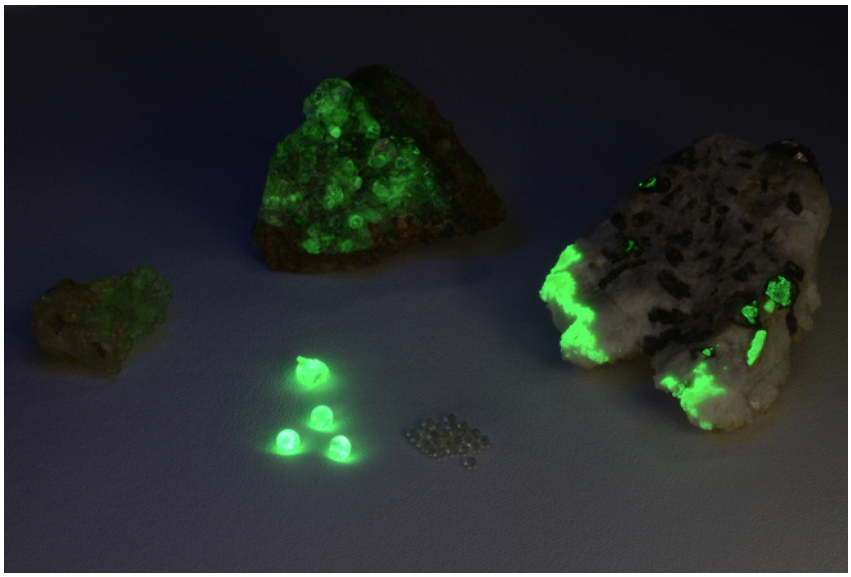

*Kazuko Saruwatari, Yusuke Katsurada, Shoko Odake, and Ahmadjan Abduriyim*

---

**Large Natural Fossil Blister PEARLS from *Tridacna* (Giant Clam) Species**

Fossil pearls, first mentioned in 1723 in John Woodward's "An essay towards a natural history of the earth and terrestrial bodies," were described in greater detail by R. Bullen Newton in 1908 ("Fossil pearl-growths," *Journal of Molluscan Studies*, Vol. 8, pp.

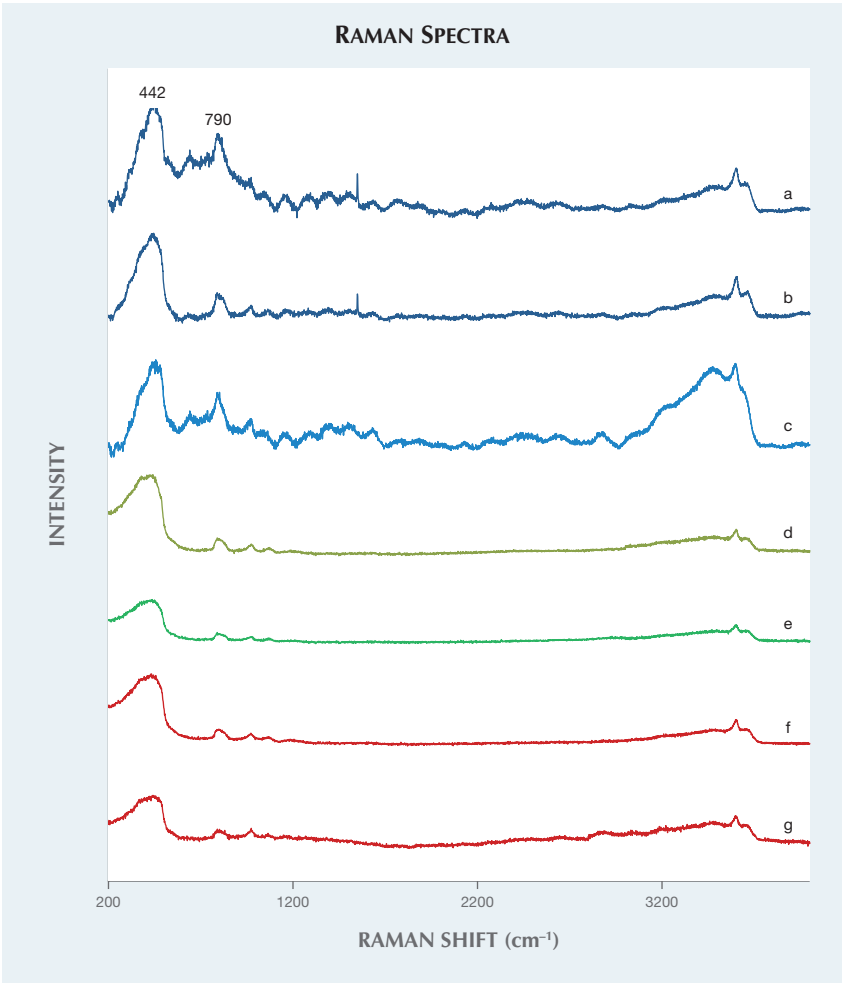


*Figure 11. Raman spectra from (a–b) Mexican hyalites, (c) Japanese pegmatitic hyalite, (d) Hungarian hyalite, (e) Argentinean hyalite, and (f–g) Japanese spherical hyalite. All spectra show similar patterns, with the Mexican specimens showing the unknown specific peak at 1548 cm$^{-1}$.*

*Figure 12. Two natural fossil blister pearls attached to their giant clam host, courtesy of Volker Bassen London Auction Rooms.*

318–320). It is a rare occurrence to receive such pearls at GIA, which is why two large fossil blister pearls recently submitted to the New York laboratory immediately caught our attention.

According to the client, the pair of fossil blister pearls were found near Lunga Lunga, a region in southeastern Kenya bordering Tanzania. They were found attached to a fossilized giant clam shell that weighed approximately 297 kg and was discovered 4.3 meters below ground (figure 12) along with some fossilized corals. The shell, along with the attached pearls, was presented to the client as a gift from a local Digo tribe. It took a month to remove the entire shell from the ground. Similar fossilized giant clam shells have been recovered from areas along the Kenyan coastline (G. Accordi et al., "The raised coral reef complex of the Kenyan coast: *Tridacna gigas* U-series dates and geological implications," *Journal of African Earth Sciences*, Vol. 58, No. 10, 2010, pp. 97–114). These two blister pearls were subsequently removed from the shell and submitted to GIA for identification after cleaning and removing the outermost fossilized debris.

The blister pearls measured approximately 58 × 47 × 45 mm and 85 × 70 × 46 mm and weighed 758 ct and 1256 ct, respectively. The faces of these pearls had a porcelaneous appearance and were smoother than the bases, which were attached to the clam shell. These bases showed chalky rough surfaces and flared forms (figure 13). Numerous natural indentations and cavities were present on their surfaces. In some areas, subtle flame-like structures were also observed at 10× magnification with the use of fiber-optic lighting (figure 14). Microradiography was not helpful owing to the specimens' sizes, but Raman spectroscopy was able to detect calcite on both specimens and aragonite on the larger pearl, although it is possible there was aragonite in untested areas on the small pearl. The presence of aragonite in the larger pearl indicates that some of those structures had been replaced by calcite during fossilization.

According to the client, the shell in figure 12 was found in the upper layers of secondary fossil reef buildup, suggesting that it lived there during the later Pleistocene period. To the authors, the shell looks similar to that of the present-day *Tridacna gigas* giant clam, but the client stated that the clam was a precursor called *Tridacna gigantea*. The large size of

*Figure 13. The two natural fossil blister pearls after removal from the giant clam shell. The left image shows the face-up view, while the right image shows the base of the pearls, where the clam shell was previously attached.*

these fossil blister pearls, their unique appearance, and the story behind their discovery proved fascinating, and offered valuable gemological and scientific information for future reference.

*Chunhui Zhou and Joyce Wing Yan Ho*

### A Natural Pearl with an Intriguing Internal Structure

Aspects of natural pearl formation remain a mystery in many cases; however, one generally accepted principle is that an intruder finds its way into the mantle or gill areas of a mollusk and instigates the pearl formation process. Gemologists are never sure what they will find when natural pearls are examined using microradiography. Substantial real-time X-ray microradiography (RTX) work by GIA staff in various locations has shown evidence of formation cause in only a few pearls.

Early in 2015, a cream semi-baroque button pearl measuring 5.22 × 5.04 mm and weighing 0.95 ct (figure 15) was submitted to GIA's Bangkok laboratory with nine other pearls. Externally the pearl appeared similar to many other previously examined natural pearls, but the microradiography uncovered something that was far from normal.

After initial RTX examination, the apparent initiator of this specimen's formation was found to be very different from anything encountered, to our knowledge, in a natural pearl. RTX revealed an attractive radiating structure within a central conchiolin-rich boundary and associated external arcs within the surrounding nacreous overgrowth (figure 16). The radial object displayed clear solid arms extending from the central core of the structure. Given the nature of the core, further investigation was performed in order to identify the radial feature and see whether the pearl was natural or formed via human intervention using an organic nucleus as a "bead."

Computed microtomography (μ-CT) analysis was used to perform a 3-D examination of the radial feature. The μ-CT results revealed a magnificent structure with a snowflake-like

*Figure 14. Porcelaneous and flame-like structures, seen here on the surface of the larger fossil blister pearl, were observed in some areas under fiber-optic lighting. Field of view 15 mm.*

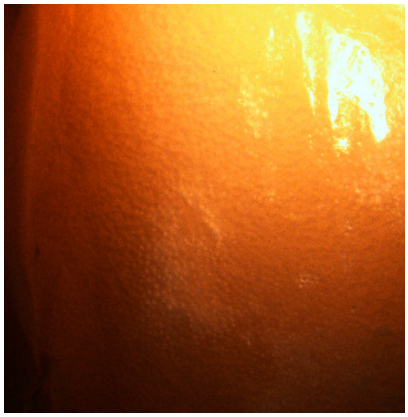

*Figure 15. The 0.95 ct pearl measuring 5.22 × 5.04 mm is shown with a GIA triplet loupe for scale.*

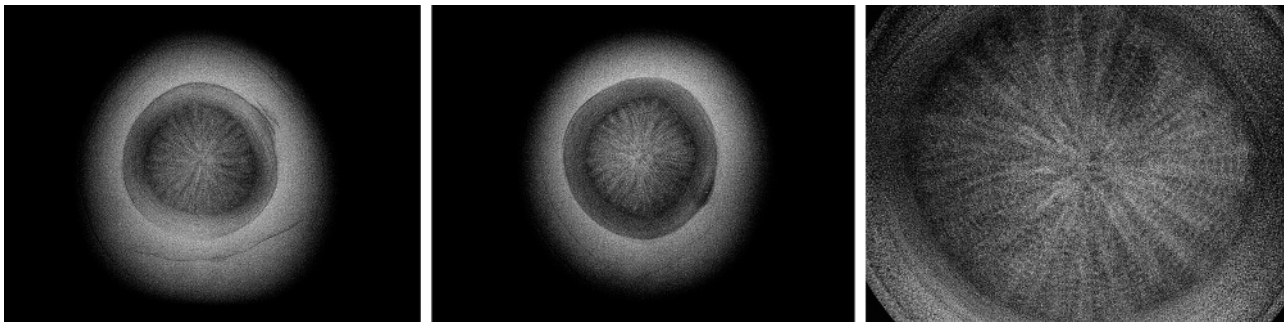

*Figure 16. The RTX images of the pearl's structure (left and right viewed from the side; center viewed from the top) revealed an intricate feature that might be an example of a foraminifera. The central feature measures approximately 1.95 × 1.93 mm, as determined by RTX and µ-CT.*

intricacy to its form (figure 17). The structure created some doubts about the natural formation of the pearl. The dark organic/conchiolin-rich growth structure, with some gaps between the nucleus and the surrounding nacre, has been noted in other unusual natural pearls of known origin. This differs from the so-called "atypical bead-cultured pearls" that almost always display a tight structure (lacking growth arcs) around the inserted nucleus. Almost all of the whole shell nuclei experimentally inserted into *Pinctada maxima* hosts have shown the boundary of the shell/nacre interface to merge tightly with one another, with very little in the way of organic arcs within the surrounding nacre. This curious structure led to further investigations into published claims of natural organic nuclei within natural pearls.

Similar but not identical structures have been documented in RTX and µ-CT work carried out on two pearls recovered from natural *P. maxima* shells by GIA staff ("An expert's journey into the world of Australian pearling," 2014, www.gia.edu/gia-news-press/malaysia-jewellery-fair). Pearls with unique structures have also been reported by others (K. Scarratt et al., "Natural pearls from Australian *Pinctada maxima*," Winter 2012 *G&G*, pp. 236–261). The exact origin of the pearls studied in Scarratt et al. is unclear, although they are more likely to be natural in at least two of the examples cited. For instance, the whole shell of one sample mentioned by Scarratt et al. showed characteristics similar to the specimen described here, with visible arcs within the nacre surrounding a shell nucleus that has a notable void/organic interface between the shell and nacre. The very small drill hole present in the shell, as opposed to the larger drill holes commonly found in cultured pearls, also strongly suggests a natural origin.

The nucleus of the 0.95 ct pearl under discussion appeared to be an organism such as coral. In order to find a match, coral samples were analyzed by RTX and µ-CT methods to compare their structures. Results indicated that the feature within the pearl may well be coral, but no exact match was noted. During the recent International Gemmological Conference (IGC) in Vilnius, Lithuania, it was suggested that the similar internal feature of a different pearl (N. Sturman et. al, "X-ray computed microtomography (µ-CT) structures of known natural and non-bead cultured *Pinctada maxima* pearls," *Proceedings of 34th International Gemmological Conference*, 2015, pp. 121–124) could well be a re-

*Figure 17. The µ-CT images reveal the structure in even more detail. Here, the nature of the organic-looking natural core is shown in three different µ-CT slices in the three different directions examined.*

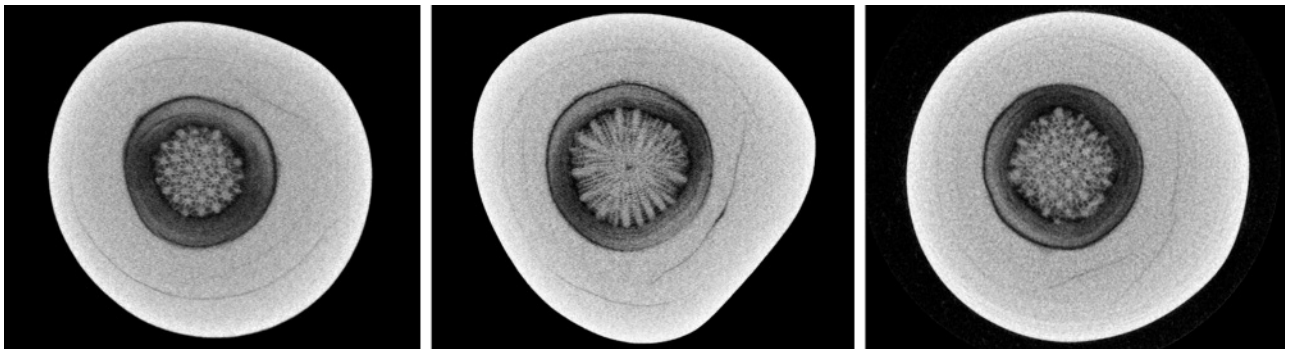

markably preserved foraminifera, a marine micro-skeleton member of a phylum of amoeboid protists. They are usually less than 1 mm in size; their structures vary, and many live on the sea floor. Given the environment, size, and features evident in the form within the pearl under discussion, it may well be that the internal structure is a type of foraminifera sphere with a porous structure for passive filtration (see figure 6 at www.mdpi.com/1660-3397/12/5/2877/html). The µ-CT results revealed the interconnecting channels and radial structure characteristic of these spherical foraminifera.

Whatever the true nature of the central form, the author considers the structure of this pearl to be natural based on the characteristics noted. It is also interesting to see that this pearl was small and not of particularly fine quality, other characteristics of natural pearl samples collected from the field. GIA's own experiments with small pieces of shell and coral using *P. maxima* hosts have produced larger pearls with different external appearances and generally finer quality than the specimen studied here. Further research into the differences between unusual structures in natural and atypical bead-cultured pearls will continue.

*Nanthaporn Somsa-ard*

*Figure 18. Left: A large natural pearl reportedly from a* Spondylus *species. Right: A large natural pearl reportedly from a* Trochoidea *species. Courtesy of Sunghee Caccavo.*

## Two Large Natural Pearls Reportedly from *Spondylus* and *Trochoidea* Species Mollusks

In a Fall 2014 Lab Note (pp. 241–242), GIA reported on four natural pearls ranging from 5.72 to 12.40 ct that were reportedly from a *Spondylus* (thorny oyster) species. These interesting non-nacreous pearls showed porcelaneous surfaces with unique bluish flame structures. Another even larger natural pearl, also reportedly from a *Spondylus* species, was recently submitted to the New York laboratory for identification. This pearl measured approximately 24 × 16 mm and weighed 42.96 ct (figure 18, left). It was formed in an attractive drop shape with a homogeneous yellow-brown bodycolor, abundant surface grooves, and a distinct bluish flame structure (figure 19). As with previous examples, microradiography showed only a tight structure, lacking obvious growth arcs. In addition, aragonite and natural polyenic pigment peaks were detected by Raman spectroscopy. Its unique appearance, coloration, and bluish tinted flame structures consistent with *Spondylus* pearls we previously reported. There is no known cultured pearl from this species, and the tight structure is commonly seen in other non-nacreous pearls, which further confirmed its natural origin.

The same client also submitted a large natural nacreous pearl reportedly from an unknown *Trochoidea* (turban snail) species (figure 18, right). The specimen, which measured approximately 27 × 19 × 12 mm and weighed 39.30 ct, had a cream color, high luster, and strong orient. Its smooth surface showed a unique wavy pattern. Previously GIA reported on a natural pearl from the turban snail species *Astraea undosa* that also showed high luster and strong iridescent colors, with an undulating wave-like pattern (Winter 2003 GNI, pp. 332–334). Both pearls share many common characteristics, and their appearances closely resemble one another.

Our client claimed that the *Spondylus* pearl is from Baja, Mexico; the turban pearl is from Mexico's Pacific coast. Although it is extremely challenging to identify the exact mollusk species these rare pearls originated from, their unique and interesting appearances are consistent with previously studied materials of similar claims. Regardless of their

*Figure 19. Distinct bluish flame structures were observed on this large non-nacreous pearl, similar to previously studied samples that also reportedly formed within* Spondylus *(thorny) oysters. Field of view 7.9 mm.*

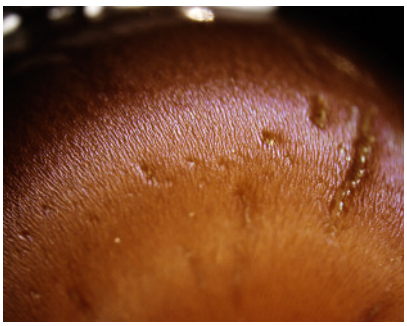

exact origin, these beautiful large natural pearls prove just how wonderful Mother Nature is at creating spectacular wonders of great variety and eye-pleasing form.

*Chunhui Zhou and Joyce Wing Yan Ho*

## Two Large CVD-Grown SYNTHETIC DIAMONDS Tested

The quality and size of near-colorless and colorless synthetic diamonds grown by chemical vapor deposition (CVD) have rapidly improved in recent years due to advances in growth techniques and the introduction of post-growth decolorizing treatments. Near-colorless CVD synthetics have now passed the three-carat threshold. In September 2015, a 3.09 ct sample (I color, $VS_2$ clarity) of unknown provenance was submitted to HRD Antwerp (www.hrdantwerp.com/en/news/hrd-antwerp-recently-examined-a-309-ct-cvd-lab-grown-diamon). This was preceded by Pure Grown Diamonds' announcement of a 3.04 ct synthetic (I color, $SI_1$ clarity) in December 2014 (www.businesswire.com/news/home/20141229005491/en/ADDING-MULTIMEDIA-Worlds-Largest-Laboratory-Pure-Grown#.VOtnbS63raQ).

GIA's New York laboratory recently tested two large CVD synthetic diamonds (figure 20) submitted for grading services. These synthetics, weighing 2.51 and 3.23 ct, are the largest CVD-grown diamonds GIA has examined to date. The results of the examination underscore the continued improvements in CVD synthetic diamonds.

The 2.51 and 3.23 ct round brilliants received H and I color grades, respectively. Microscopic examination revealed pinpoint and black inclusions in both, while small fractures along the girdle were only observed in the 2.51 ct round (figure 21). The 3.23 ct synthetic contained a small black inclusion measuring approximately 125 µm. As a result, $SI_1$ and $VS_2$ clarity grades were given to the 2.51 and 3.23 ct samples, respectively. Both revealed irregular stress patterns with high-order interference colors when viewed under cross-polarized light (figure 22), indicating high levels of strain.

*Figure 20. The I-color 3.23 ct round on the left (9.59–9.61 × 5.83 mm) and H-color 2.51 ct round on the right (8.54–8.56 × 5.43 mm) are the largest CVD synthetic diamonds GIA has tested.*

The synthetics showed weak orange fluorescence to conventional short-wave UV and were inert to long-wave UV radiation. Exposure to the deep UV radiation (< 230 nm) of the DiamondView revealed an overall strong red-pink fluorescence attributed to nitrogen-vacancy centers with dislocation bundles that fluoresced violet-blue (figure 23), followed by weak greenish blue phosphorescence. Both samples were characterized by a layered growth structure, suggesting that the crystals were grown using a multi-step technique to maximize their volume. The sharp boundaries between the different growth layers are a result of changes in the fluorescent impurity uptake during the starting, stopping,

*Figure 21. Left: These pinpoint inclusions were observed in the 2.51 ct synthetic diamond. Right: A small black inclusion measuring approximately 125 µm was observed in the 3.23 ct sample. Field of view 4.72 mm (left) and 6.27 mm (right).*

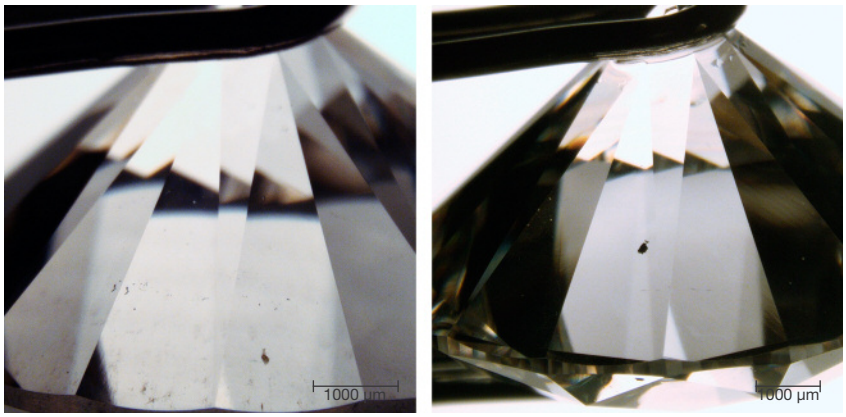

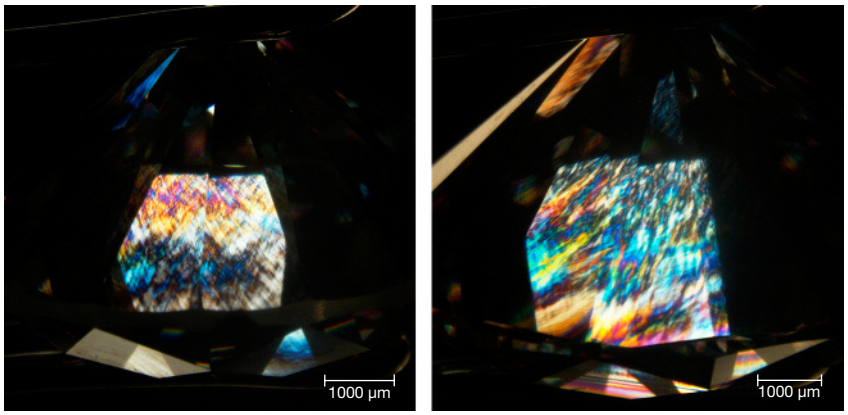


*Figure 22. Irregular stress patterns were observed under the microscope with cross-polarized light. Both the 2.51 ct (left) and 3.23 ct (right) synthetic diamonds showed high-order interference colors. Field of view 5.76 mm and 6.27 mm, respectively.*

and restarting of growth. These images clearly revealed that at least five growth layers were applied to produce these large crystals. The patterns suggest that the table of the 2.51 ct sample was cut parallel to the growth layers, while the table of the 3.23 ct synthetic was cut at an angle to the growth layers. The dislocation bundles are seen to propagate through the different growth layers. The formation of the two blue bands of highly concentrated dislocations crossing the table of the 2.51 ct specimen is not understood.

Infrared absorption spectroscopy in the mid-IR range (6000–400 $cm^{-1}$) showed no major nitrogen-related absorption in the one-phonon region, which classified both samples as type IIa. No hydrogen-related defects were detected, either. UV-Vis-NIR absorption spectra collected at liquid-nitrogen temperature revealed a smooth increase in absorption from the infrared region to the high-energy end of the spectrum, with a 737 nm peak in both samples and a small absorption peak at 596 nm in the 3.23 ct synthetic. The 737 nm peak is an unresolved doublet at 736.6/736.9 nm attributed to $[SiV]^-$. This center is often inadvertently introduced during CVD growth (P. Martineau et al., "Identification of synthetic diamond grown using chemical vapor deposition (CVD)," Spring 2004 *G&G*, pp. 2–25; W. Wang et al., "CVD synthetic diamonds from Gemesis Corp.," Summer 2012 *G&G*, pp. 80–97) but is rarely observed in natural diamonds, especially using absorption methods. The 596 nm feature is particularly useful for identification purposes, as it has only been reported in CVD synthetic material (again, see Martineau et al., 2004).

Photoluminescence (PL) spectra acquired with 514 nm laser excitation at liquid-nitrogen temperature revealed a doublet at 596/597 nm, nitrogen-vacancy centers at 575 $[NV]^0$ and 637 $[NV]^-$ nm, and $[SiV]^-$ at 736.6/736.9 nm for both samples, with the $[NV]^{0/-}$ luminescence dominating. The strength of the $[NV]^{0/-}$ centers was consistent with the red-pink fluorescence colors (figure 23). Although the 596/597 nm doublet is not thought to arise from the same center as the 596 nm feature seen in the absorption spectrum of the 3.23 ct sample, it has only been detected in CVD synthetics, thus revealing the samples' CVD origin (Martineau et al., 2004). The doublet also indicated that the samples had not undergone post-growth HPHT (high-pressure, high-temperature) processing to improve their color, as the treatment would have removed this feature.

*Figure 23. DiamondView imaging of both samples revealed strong red-pink fluorescence superimposed with dislocation patterns that fluoresced violet-blue. A layered growth structure indicating start-stop growth was clearly observed on the pavilion of both. The orientation of the layers reveals that the 2.51 ct sample (top) was cut with its table approximately parallel to the growth plane, whereas the layers intersect the table facet in the 3.23 ct sample (bottom).*

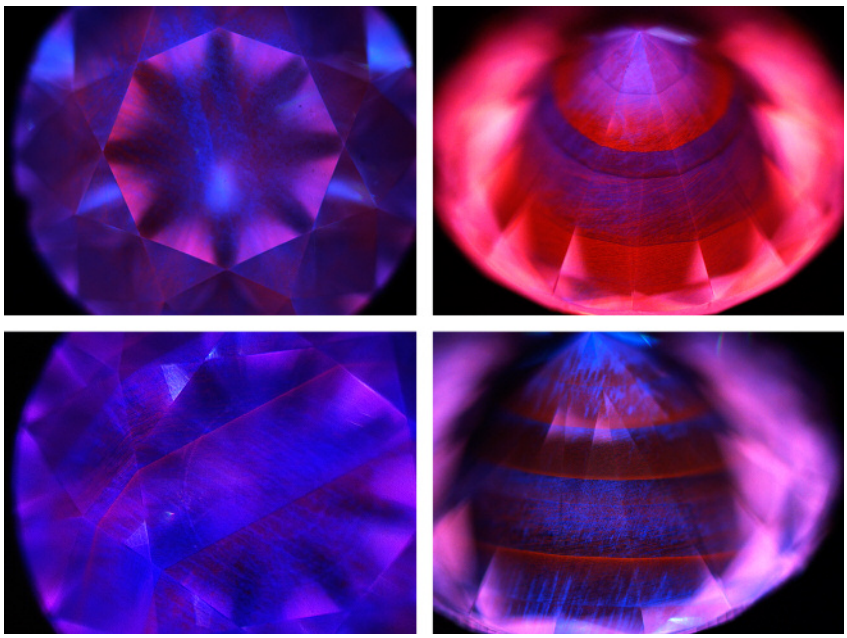

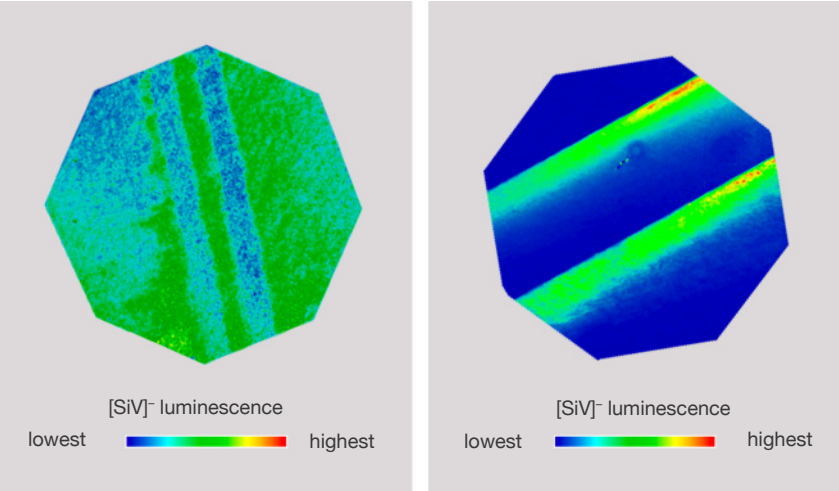


*Figure 24. PL [SiV]⁻ silicon distribution maps were collected with 532 nm laser excitation. Left: Less luminescence from [SiV]⁻ centers is observed in two broad bands on the 2.51 ct sample. Right: More intense [SiV]⁻ luminescence is found at the diamond layer boundaries in the 3.23 ct sample.*

The distribution of [SiV]⁻ centers was investigated through PL mapping of the 736.6/736.9 nm doublet at liquid-nitrogen temperature using 532 nm laser excitation (figure 24). The distribution was different between the two samples, forming patterns that corresponded directly with their DiamondView images (again, see figure 23). For the 2.51 ct sample, the [SiV]⁻ luminescence decreased along the bands with higher concentrations of dislocation bundles. This may indicate that there are fewer [SiV]⁻ centers in this region, or an increased concentration of defects (either structural or impurity-based) that effectively quench the [SiV]⁻ luminescence. Where the growth layers intersect the table in the 3.23 ct sample, the [SiV]⁻ luminescence appeared to be highest at the start of a layer's growth, decreasing as the growth progressed. This could mean that the concentration of silicon in the growth gas fell over time, or that the concentration of defects that may quench the [SiV]⁻ luminescence increased during growth. Notably, the concentration of dislocations increased as growth progressed.

Analysis of these two large samples demonstrates that high-quality CVD synthetic diamonds can be produced even without post-growth decolorizing HPHT treatment, marking a significant improvement in CVD growth. Using advanced spectroscopic and fluorescence imaging technologies, it is nevertheless possible to detect low concentrations of impurity centers, allowing conclusive determination of these samples' synthetic origin. GIA is monitoring the development of laboratory-grown diamonds and conducting research to ensure that we can continue identifying every single synthetic diamond.

*Caitlin Dieck, Lorne Loudin, and Ulrika D'Haenens-Johansson*

## SYNTHETIC ROCK CRYSTAL QUARTZ Bangle with Unusual Inclusions

Synthetic quartz is grown by the hydrothermal technique, which can produce large single crystals of high quality (K. Byrappa and M. Yoshimura, *Handbook of Hydrothermal Technology: A Technology for Crystal Growth and Material Processing*, William Andrew Publishing, 2001). This process, widely used in the jewelry trade, has led to difficulty in separating synthetic quartz from its natural counterpart (R. Crowningshield et al., "A simple procedure to separate natural from synthetic amethyst on the basis of twinning," Fall 1986 *G&G*, pp. 130–139). The presence of Brazil-law twinning and certain inclusions, such as tourmaline or golden rutile needles, can be used to distinguish natural from synthetic quartz. But high-quality quartz, whether of natural or synthetic origin, typically has no inclusions or twinning. In this case, standard gemological testing may not be able to identify the origin. Advanced instruments, including infrared absorption spectroscopy (S. Karampelas et al., "An update in the separation of natural from synthetic amethyst," *Bulletin of the Geological Society of Greece*, 2007, pp. 805–814) and LA-ICP-MS are considered useful tools for separating natural from synthetic material from material with synthetic origins (C.M. Breeding, "Using LA-ICP-MS analysis for the separation of natural and synthetic amethyst and citrine," *GIA News from Research*, 2009, www.gia.edu/gia-news-research-nr73109a).

The Bangkok lab recently examined a high-clarity, transparent, near-colorless bangle (figure 25). Standard gemological testing revealed a spot RI of 1.54 and an SG of 2.65, consistent with quartz. Magnification revealed irregular two-phase inclusions (figure 26). These inclusions are more likely to be present in natural quartz than in

*Figure 25. A synthetic rock crystal quartz bangle measuring approximately 80 × 22 × 10 mm.*

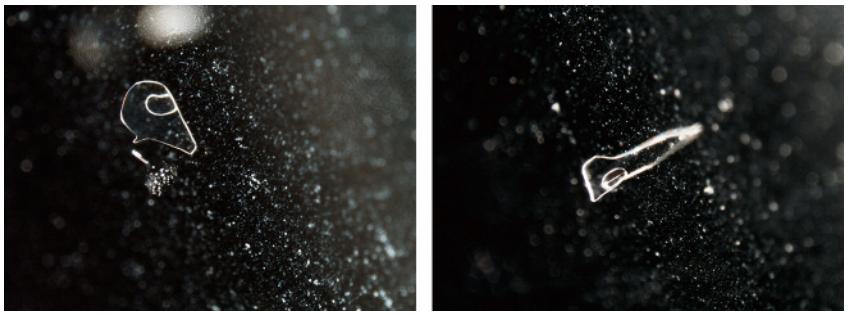

*Figure 26. Irregular two-phase inclusions seen in the bangle using dark-field illumination (left and right) are similar to those found in natural specimens but are rarely found in hydrothermal synthetic quartz. Field of view 4.1 mm.*

hydrothermal synthetic quartz, which typically shows nail-head spicule and breadcrumb inclusions. This bangle also gave an IR absorption spectrum unlike that of natural rock crystal quartz. The characteristic IR absorptions of natural rock crystal quartz occurred at 3379, 3483, and 3595 $cm^{-1}$. These features are never seen in synthetic rock crystal quartz. The IR spectrum of the bangle showed absorption peaks at 3610, 3585, 3431, 3294, and 3194 $cm^{-1}$ (figure 27), which matches the IR absorption features of synthetic rock crystal quartz (P. Zecchini and M. Smaali, "Identification de l'origine naturelle ou artificielle des quartz," *Revue de Gemmologie*, No. 138/139, 1999, pp. 74–80). The IR spectrum confirmed that this material was grown by hydrothermal methods.

*Figure 27. Infrared spectra of the synthetic rock crystal quartz bangle and a 17.50 ct natural rock crystal quartz faceted bead show different absorption patterns. The characteristic absorptions of natural rock crystal quartz at 3379, 3483, and 3595 $cm^{-1}$ are never seen in synthetic rock crystal quartz. The bangle showed absorption peaks at 3610, 3585, 3431, 3294, and 3194 $cm^{-1}$, matching the IR absorption of synthetic rock crystal quartz.*

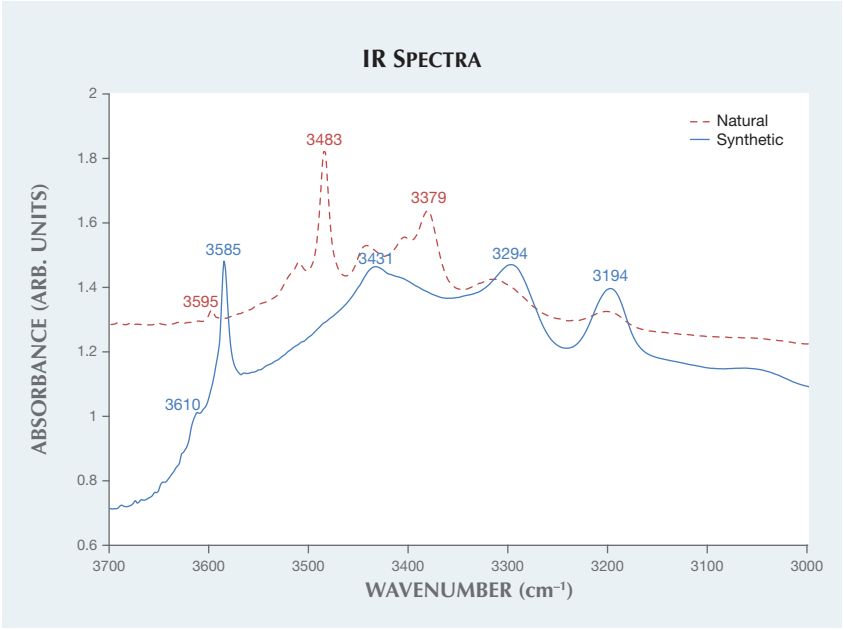


Large transparent colorless quartz can be found in natural and synthetic forms, but synthetic quartz is usually seen as a flat crystal. This bangle is an interesting example of large, high-clarity synthetic quartz used in jewelry. The presence of the irregular two-phase inclusions in this example serves as an important reminder that natural and synthetic quartz can show a similar appearance and contain internal inclusion features that are identical.

*Nattida Ng-Pooresatien*

*PHOTO CREDITS:*
*Jian Xin (Jae) Liao—1, 7, 20; Yixin (Jessie) Zhou— 2; Sood Oil (Judy) Chia—4, 13, 18; Kyaw Soe Moe—5, 6; Masumi Saito—9, 10; Joyce Wing Yan Ho—14, 19; Caitlin Dieck—21, 22, and 23; Lorne Loudin—24; Nuttapol Kitdee—25; Nattida Ng-Pooresatien—26.*